JACS
JOURNAL OF THE AMERICAN CHEMICAL SOCIETY

COMMUNICATION

pubs.acs.org/JACS

Detection of Single Nucleotide Polymorphism Using Tension-Dependent Stochastic Behavior of a Single-Molecule Template

Deepak Koirala, Zhongbo Yu, Soma Dhakal, and Hanbin Mao

Department of Chemistry and Biochemistry, Kent State University, Kent, Ohio 44242, United States

Supporting Information

ABSTRACT: Single nucleotide polymorphism (SNP) is the most common genetic variation among individuals. The association of SNP with individual's response to pathogens, phenotypic variations, and gene functions emphasizes the importance of sensitive and reliable SNP detection for biomedical diagnosis and therapy. To increase sensitivity, most approaches employ amplification steps, such as PCR, to generate detectable signals that are usually ensemble-averaged. Introduction of amplification steps increases the complexity of a system, whereas ensemble averaging of signals often suffers from background interference. Here, we have exploited the stochastic behavior of a single-molecule probe to recognize SNP sequence in a microfluidic platform using a laser-tweezers instrument. The detection relies on on−off mechanical signals that provide little background interference and high specificity between wild type and SNP sequences. The microfluidic setting allows multiplex sensing and in situ recycling of the SNP probe. As a proof-of-concept, we have detected as low as 100 pM of an SNP target associated with coronary heart diseases within half an hour without any amplification steps. The mechanical signal permits the detection of single mutations involving either G/C or A/T pairs. We anticipate this system has the capacity to function as a highly sensitive generic biosensor after incorporation of a specific recognition element, such as an aptamer for example.

Single nucleotide polymorphism (SNP) is a common genetic variation in human genome with an average occurrence of ~1/1000 base pairs.[1] SNP detection is crucial for biological and clinical aspects since SNP is associated with diseases, anthropometric characteristics, phenotypic variations, and gene functions.[2] Recent strides toward personalized medicine necessitate the recognition of genetic markers to track diseases, which further amplifies the importance of SNP detection.

Most SNP-detecting methods use amplification steps such as PCR to achieve highly sensitive detection. However, efficiency of PCR is dependent on the sequence of a target. Recently, Mirkin and co-workers[3] developed alternative nanoparticle-based amplifications and attained femtomolar detection limits. Methods incorporating amplification steps require laborious and time-consuming multistep protocols, which may expose a sample to uncontrollable human and environmental factors. Fluorescence-based approaches, such as molecular beacon,[4] employ fewer amplification steps to reduce these disadvantages. Yet, fluorescence signals often suffer from endogenous background that deteriorates detection limit. To minimize sophisticated amplification steps while achieving superior detection limit, herein we report a force-based sensing of SNP at the single-molecule level. The single-molecule nature presents superior sensitivity with an inherent capacity for stochastic sensing.[5] Compared to fluorescence signal, mechanical signal has little environmental interference. The on−off mechanical signals of a single DNA template that recognizes SNP are recorded by laser tweezers[6] in a microfluidic platform. Although previous attempts to combine laser tweezers and lab-on-a-chip system exist,[7] our method represents the first SNP sensing based on these two techniques.

Figure 1 shows the sensing scheme. A hairpin that contains SNP recognition sequence serves as a probe, which is sandwiched between two dsDNA handles separately anchored to two optically trapped beads. The proof-of-concept SNP (SNP Rs1333049) we selected has been associated with coronary heart diseases.[2a,g] The tethered SNP probe was placed inside a microfluidic device with interconnected channels (Figure 1D and Supporting Information Figure S1). This design allows desired buffers in separate channels while keeping free movement of the SNP probe between channels. Before sensing, the tethered DNA construct was repeatedly stretched and relaxed, which allowed unfolding and refolding of the hairpin[8] in the SNP probe, respectively (Figure 2A). Hopping between folded, or "on", and unfolded, or "off", states of the hairpin was also observed at fixed positions of the two laser traps (Figure 2B). Analysis of the change in contour length and rupture force confirmed the hairpin structure in the DNA construct (Supporting Information Figure S2).

In our first design of a SNP probe, each end of the 19-nt probe extends 2-nt into the hairpin stem (hairpin 1 in Figure 1B). The distance between the two laser traps was adjusted to allow the bistate stochastic hopping of the hairpin in the buffer channel (Figure 2B, top panel). This on−off behavior was exploited for subsequent detection of oligodeoxynucleotide (ODN) targets. When the SNP probe was moved to the channel that contains a complementary 19-nt ODN (CMP1 in Figure 1C) with 1 μM concentration, hopping immediately ceased and the hairpin populated in its unfolded state (Figure 2B, bottom panel). In contrast, hopping of the hairpin persisted for up to 35 min in the presence of a noncomplementary ODN (NCMP in Figure 1C). These observations were consistent with the specific binding of

Received: March 3, 2011
Published: June 03, 2011

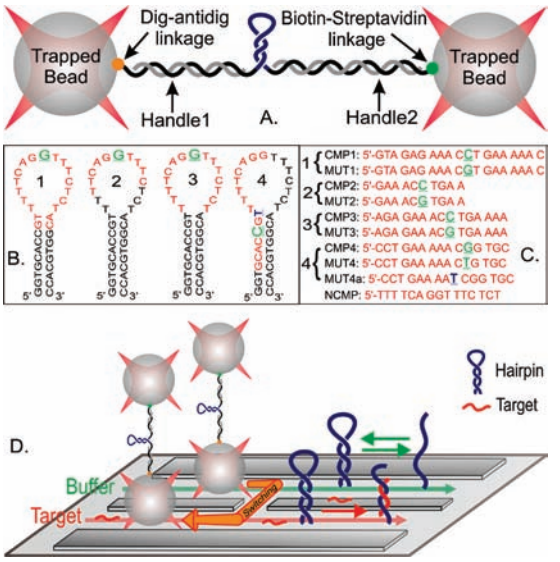

Figure 1. Schematic of sensing strategy. (A) The SNP probe contains a hairpin that recognizes specific DNA sequences. The hairpin is sandwiched between two dsDNA handles, which are tethered to two optically trapped beads via digoxigenin (Dig)−antiDig antibody and biotin−streptavidin linkages, respectively. (B) Hairpins used for four sensing strategies with recognition sites (red) for (C) four sets of wild-type (CMP) and SNP (MUT) targets. NCMP is the control DNA target. Single mutation sites are indicated with corresponding colors in B and C. (D) Sensing mechanism for the SNP probe. The buffer channel (top) hosts the DNA construct that hops between folded and unfolded hairpin states. As depicted by the orange arrow, this DNA construct then moves via the conduit to the target channel (bottom) in which a DNA target is present. The specific recognition between the SNP probe and the target terminates the hopping of the hairpin.

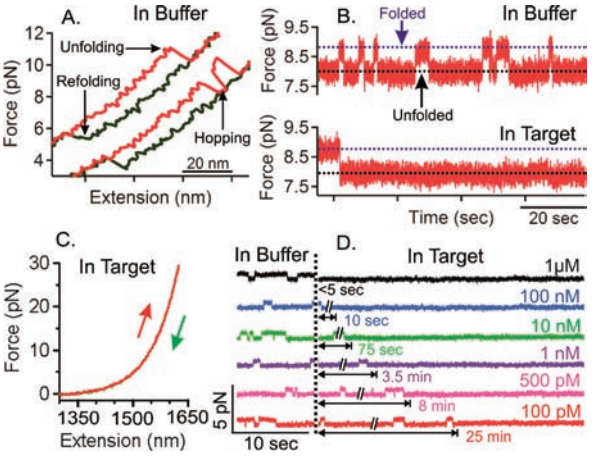

Figure 2. Detection of CMP1 by stochastic hairpin hopping. (A) Typical F−X curves during the mechanical stretching (red) and relaxing (green) of the SNP probe in the buffer channel. (B) Force vs time traces observed for the SNP probe at fixed optical trap positions in the buffer (top) and the target (bottom) channel. (C) F−X curves of the SNP probe in the target channel where folding/unfolding features were not observed. (D) Hopping traces for SNP probe with different CMP1 concentrations. The vertical dotted line indicates the transfer of the SNP probe from the buffer to the target channel. Double-headed arrows depict the average time observed before the hopping ceases to the unfolded hairpin state, which indicates the binding of the CMP1 to the hairpin.

the CMP1 to the probe, which eliminated the hopping. The specific binding was further supported by the absence of unfolding and refolding features in the force extension (F−X) curves in the presence of CMP1 (Figure 2C); while these features were not affected in 1 μM NCMP solutions (data not shown).

To facilitate the binding of CMP1, we varied the concentration of CMP1 under the trap-to-trap distance that favored unfolded hairpin. As shown in Figure 2D, the average time required to catch a CMP1 molecule (indicated by double-headed arrows) was inversely dependent on the CMP1 concentration (see Supporting Information Figure S4 for a distribution of time intervals). Given enough time, it was expected to detect much lower concentration of the CMP1. However, due to the limit of the effective detection area vs cross-section of the microfluidic channel ($\sim$50 nm^2 vs 100,000 μm^2, see below), we were able to detect 100 pM targets in 30 min. Surprisingly, when an SNP sequence (MUT1, Figure 1C) was tested, similar binding behavior and detection limit were observed (data not shown).

To distinguish the binding of MUT1 from CMP1, we applied a force up to 60 pN on the hairpin bound with either of the two targets in the buffer channel. During this process, we observed a small rupture event at the force above 25 pN (Figure 3A). When the tension was relaxed, the refolding of the hairpin was almost always observed at the lower force region (<10 pN, Figure 3A). We surmise the rupture event represents the ejection of the bound target probably due to the force-induced melting.[9] The observed change in contour length (ΔL) of the ejection events matches well with the value calculated when bound DNA target is lost (see Supporting Information Figure S3). The ejection of bound targets, therefore, forebodes the regeneration of the SNP probe at the lower force range. When we compared the ejection forces for CMP1 and MUT1, we found the former required significantly higher value than the latter (44 $\pm$ 1 pN vs 36 $\pm$ 1 pN, Figure 3B). "Force titration" experiments in which maximal extending forces were increased 5 pN each time were performed to estimate the probability of ejection (or regeneration) in each force range. The result (Figure 3C) was identical with that obtained by the integration of the histograms in Figure 3B. Based on the 50% ejection probability, we calculated the selectivity between CMP1 and MUT1 as 80:1 (Defined as detection of one CMP1 in the presence of 80 MUT1 molecules, see Supporting Information for details).

To increase the specificity, we selected shorter DNA targets with the expectation that single site mutation will be more pronounced. However, binding was not observed for 10-nt targets (CMP2 and MUT2, Figure 1C) at the concentration as high as 10 μM. For 15-nt sequences (CMP3 and MUT3, Figure 1C), target binding that prevents the hopping of the hairpin in the SNP probe only occurred at the concentration above 100 nM.

To optimize between the specificity and the binding strength, we selected 15-nt sequences (CMP4 and MUT4, Figure 1C) that recognize both the stem and the loop of the hairpin probe (hairpin 4 in Figure 1B). This strategy demonstrated dramatic improvement in the detection limit and the selectivity. The ejection force analysis showed that the probe bound with CMP4 required 43 $\pm$ 1 pN, whereas that with MUT4 required 30 $\pm$ 2 pN to eject the target (Figure 4A). The difference between these two ejection forces (13 $\pm$ 2 pN) is significantly higher than that for the 19-nt targets (8 $\pm$ 1 pN). The analysis on the regeneration probability also demonstrated increased difference between these two targets at specific force (Figure 4B). To evaluate the

dx.doi.org/10.1021/ja201976r | J. Am. Chem. Soc. 2011, 133, 9988–9991

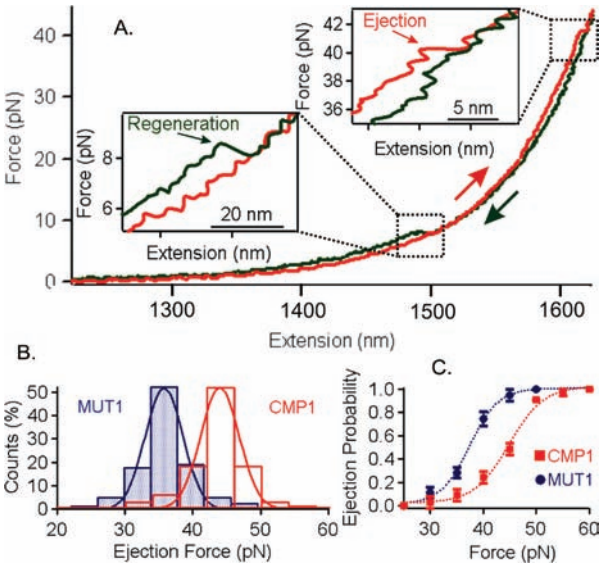

Figure 3. Differentiation of CMP1 and MUT1. (A) Typical F−X curves for CMP1 or MUT1 bound SNP probe. The red and green arrows represent the stretching and relaxing curves, respectively. The right inset shows a feature due to the ejection of the bound target. The left inset shows the refolding of the hairpin, which indicates the regeneration of the probe. (B) Histograms of ejection force for CMP1 (red) and MUT1 (blue). The solid curves are Gaussian fitting. (C) The probability of target ejection (or probe regeneration) vs template tension for CMP1 (red) and MUT1 (blue). Dotted curves are sigmoidal fitting for guidance.

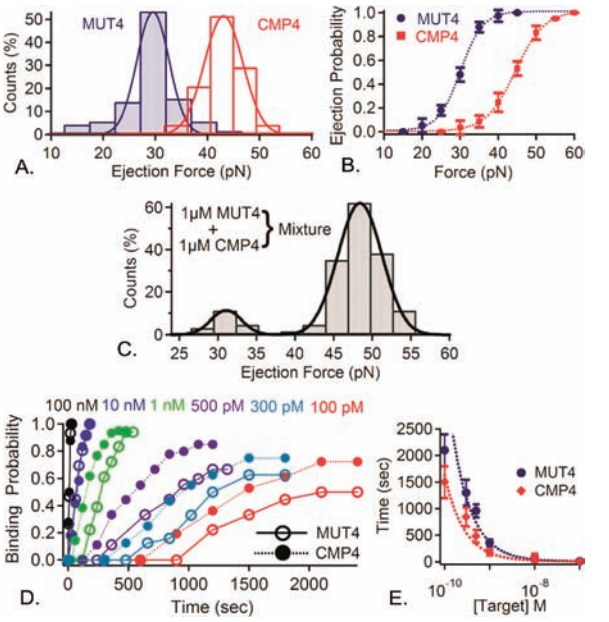

Figure 4. Optimization of selectivity in the SNP detection. (A) Histograms of ejection force for CMP4 (red) and MUT4 (blue). The solid curves are Gaussian fitting. (B) Probability of probe regeneration (or target ejection) vs template tension for CMP4 (red) and MUT4 (blue). The dotted curves are sigmoidal fitting for guidance. (C) Histogram of ejection force (black bars) for a mixture containing 1 μM each of CMP4 and MUT4. Black curve is the two-peak Gaussian fitting. (D) Probability of target binding vs detection time for CMP4 (filled circles linked by dotted lines) and MUT4 (empty circles linked by solid lines) with different concentrations. (E) Time required for CMP4 (red) and MUT4 (blue) with 50% binding probability to the SNP probe ($t_{1/2}$) under different target concentrations. Dotted curves are the fitting based on the effective area of detection ($A_{effective}$, see text).

capability of this sensing approach in a more practical setting, we exposed the SNP probe in a mixture of 1 μM each of CMP4 and MUT4. The ejection force histogram clearly showed two distinct peaks, 46 ± 2 and 30 ± 1 pN (Figure 4C), which were assigned to the CMP4 and MUT4 populations, respectively, by comparison of the known ejection forces (Figure 4A). It is noteworthy that in practice, a single ejection procedure can differentiate CMP4 or MUT4 as these two populations do not overlap (Figure 4C). Further calculation revealed a remarkably increased selectivity of 1600:1 between CMP4 and MUT4 (see Supporting Information for details).

Next, we measured the time required for the SNP probe to catch either CMP4 or MUT4. To this purpose, we adjusted the trap-to-trap distance to populate the hairpin in its unfolded state in the buffer channel. We then exposed the SNP probe to CMP4 or MUT4 in separate microfluidic channels with 100 nM-100 pM target concentrations. The binding of a specific target was revealed by the absence of hairpin refolding event in the F−X curves collected at certain time interval. The probe was regenerated at higher forces for the next round of detection. Figure 4D depicts that for concentrations below 10 nM, the binding for CMP4 takes less time compared to MUT4, indicating it is easier for the SNP probe to recognize a complementary sequence than a mutant. Assuming a diffusion-controlled target recognition process in an effective detection area of $A_{effective}$, we calculated the time for 50% probability of target binding (or half time, $t_{1/2}$) based on the rate of the target molecules that enter this area,

$$t_{1/2} = \frac{A_{total}}{2 \times v_{flow} \times C \times N_A \times A_{effective}} \quad (1)$$

where v_{flow} is the flow rate of the buffer in a microfluidic channel, C is the target concentration, N_A is the Avogadro's number, and A_{total} is the area of the cross section for the channel (see Supporting Information). This expression gave good fitting to the curves shown in Figure 4E, which reveals that the detection half time increases with decreasing target concentration. The fitting yielded $A_{effective}$ of 70 nm^2 for CMP4 and 41 nm^2 for MUT4 recognition, which is consistent with Figure 4D indicating CMP4 can be recognized more efficiently than MUT4. Equation 1 also implies that with increased flow rate and decreased size of a microfluidic channel, $t_{1/2}$ can be effectively reduced to detect targets with even lower concentrations. For example, to detect 1 fM with a $t_{1/2}$ of 30 min, which is on the order of the most sensitive detection limit for current techniques,[3] calculation from eq 1 reveals that a microfluidic channel with A_{total} of 50 μm^2 and a flow rate of 20 μL/min are required.

This sensing strategy can also detect with comparable sensitivity single A or T mutations (MUT4a, Figure 1C), which involve a loss of two instead of three hydrogen bonds as demonstrated above (see Supporting Information Figure S5 for details).

In summary, we have successfully demonstrated a novel single-molecule SNP detection method using stochastic mechanical signals. The mechanical signal with little endogenous background noise warrants superior sensitivity for this approach. The on−off state of the detector can be adjusted by control of the tension in the SNP probe, which also effects the *in situ* recycling of the sensor. The microfluidic platform allows multiplex sensing after the incorporation of additional channels. In fact, we have

dx.doi.org/10.1021/ja201976r |*J. Am. Chem. Soc.* 2011, 133, 9988–9991

successfully tested this capability in a 5-channel microfluidic device. As a proof-of-concept, we were able to detect 100 pM of an SNP target in 30 min. Given appropriate microfluidic design and optimization of the flow rate, we anticipate this method can detect much lower target concentrations within the same time frame. This technique is not only applicable to detect SNP but also amenable to serve as a generic on−off digital biosensor, by using specific recognition elements such as DNA aptamers for example.

■ ASSOCIATED CONTENT

Supporting Information. DNA construct synthesis, single-molecule experiments in the laser tweezers instrument, preparation of microfluidic platform, SNP probe characterization, procedures for the calculation of the detection time, the effective detection area, the selectivity, the analysis of mutant MUT4a, and the complete list of authors for the references,1c,1d,2c,2d and 2g. This material is available free of charge via the Internet at http://pubs.acs.org.

■ AUTHOR INFORMATION

Corresponding Author
hmao@kent.edu

■ ACKNOWLEDGMENT

We thank the New Faculty Award Program at Camille and Henry Dreyfus Foundation, a Kent State University startup, and Ohio Board of Regents for financial support.

■ REFERENCES

(1) (a) The International SNP Map Working Group *Nature* **2001**, *409*, 928−933. (b) Altshuler, D.; Pollara, V. J.; Cowles, C. R.; Van Etten, W. J.; Baldwin, J.; Linton, L.; Lander, E. S. *Nature* **2000**, *407*, 513–516. (c) Venter, J. C.; et al. *Science* **2001**, *291*, 1304–1351. (d) Wang, D. G.; et al. *Science* **1998**, *280*, 1077–1082.

(2) (a) The Wellcome Trust Case Control Consortium *Nature* **2007**, *447*, 661-678. (b) McCarthy, J. J.; Hilfiker, R. *Nat. Biotechnol.* **2000**, *18*, 505–508. (c) Frayling, T. M.; et al. *Science* **2007**, *316*, 889–894. (d) Begovich, A. B.; et al. *Am. J. Hum. Genet.* **2004**, *75*, 330–337. (e) Bond, C.; LaForge, K. S.; Tian, M.; Melia, D.; Zhang, S.; Borg, L.; Gong, J.; Schluger, J.; Strong, J. A.; Leal, S. M.; Tischfield, J. A.; Kreek, M. J.; Yu, L. *Proc. Natl. Acad. Sci U.S.A.* **1998**, *95*, 9608–9613. (f) Evans, W. E.; Relling, M. V. *Science* **1999**, *286*, 487–491. (g) Karvanen, J.; et al. *Genet. Epidemiol.* **2009**, *33*, 237–246.

(3) (a) Taton, T. A.; Mirkin, C. A.; Letsinger, R. L. *Science* **2000**, *289*, 1757–1760. (b) Nam, J.-M.; Stoeva, S. I.; Mirkin, C. A. *J. Am. Chem. Soc.* **2004**, *126*, 5932–5933.

(4) (a) Tyagi, S.; Kramer, F. R. *Nat. Biotechnol.* **1996**, *14*, 303–308. (b) Tan, W.; Wang, K.; Drake, T. J. *Curr. Opin. Chem. Biol.* **2004**, *8*, 547–553.

(5) Bayley, H.; Cremer, P. S. *Nature* **2001**, *413*, 226–230.

(6) (a) Mao, H.; Luchette, P. *Sensor Actuators B* **2008**, *129*, 764–771. (b) Yu, Z.; Schonhoft, J. D.; Dhakal, S.; Bajracharya, R.; Hegde, R.; Basu, S.; Mao, H. *J. Am. Chem. Soc.* **2009**, *131*, 1876–1882.

(7) (a) Gross, P.; Farge, G.; Peterman, E. J. G.; Wuite, G. J. L.; Nils, G. W. *Methods in Enzymology*; Academic Press: New York, 2010; Vol. 475, pp 427−453. (b) Enger, J.; Goksor, M.; Ramser, K.; Hagberg, P.; Hanstorp, D. *Lab Chip* **2004**, *4*, 196–200.

(8) (a) Liphardt, J.; Onoa, B.; Smith, S. B.; Tinoco, I.; Bustamante, C. *Science* **2001**, *292*, 733–737. (b) Woodside, M. T.; Anthony, P. C.; Behnke-Parks, W. M.; Larizadeh, K.; Herschlag, D.; Block, S. M. *Science* **2006**, *314*, 1001–1004.

(9) Williams, M. C.; Wenner, J. R.; Rouzina, I.; Bloomfield, V. A. *Biophys. J.* **2001**, *80*, 874–881.